Elastic Image Registration for Landslides Monitoring

Siti Khairunniza-Bejo[a,]*, Maria Petrou[b]
[a]*Department of Biological and Agricultural Engineering, Faculty of Engineering, Universiti Putra Malaysia, 43400 Serdang, Selangor, MALAYSIA.*
[b]*Department of Electrical and Electronic Engineering, Imperial College, London, SW7 2AZ, UK*
**Email: skbejo@eng.upm.edu.my*

Abstract

Landslide is a type of mass movement that causes damage in many areas. The evolving remote sensing technology in producing high resolution images may help in landslide studies. However, the problem in detecting small size landslides is still challenging when suitable image resolution of the area being analyzed is not available. In this paper, a novel method based on elastic image registration, appropriate for the detection of small landslides will be presented. This method can be used to detect and quantify landslide movement with sub-pixel accuracy. It is based on the invocation of deformation operators which imitate the deformations expected to be observed when a landslide occurs. The similarity between two images is measured by a similarity function which takes into consideration grey level value correlation and geometric deformation. The geometric deformation term ensures that the minimum necessary deformation compatible with the two images is employed. An extra term, ensuring maximum overlap between the two images is also incorporated. There are two versions of this method. One using the correlation coefficient as a measure of similarity for the grey level value, and another one using mutual information. These methods are tested using known small scale landslides images of southern Italy taken from the Landsat 5 TM. The mutual information-based method gives more reliable results.

Keywords: *Mathematical models; Deformation operators; Elastic image registration; Correlation coefficient; Mutual information; Landslide monitoring*

1. Introduction

Image registration methodology such as template matching, temporal, multimodal and viewpoint registration [1] has been used in landslide studies for analyzing landslide images [2, 3] obtained at different dates, by different sensors and from different viewpoints [4, 2, 5, 6, 7]. There are two types of approach for registering landslide images: those with and those without sub-pixel accuracy. In registering landslide images without sub-pixel accuracy, two images are overlapped and a set of Ground Control Points (GCPs) in both images is extracted. This set of GCPs must be features that have sharp contrast with their surrounding area and must be well distributed throughout the images. In order to correlate two homogenous GCPs, Honda and Nagai [8] and Casson et al. [9] used the correlation coefficient to calculate image similarity. In such studies, the set of points matched is used to generate a transformation function between the two images such as affine transformation and polynomial transformation. Transformation estimation algorithms for non-rigid transformation vary in their handling of local deformations. Zagorchev and Goshtasby [10] conducted a comparative study of four of the commonly used transformation functions for non-rigid transformation, namely, thin plate spline (TPS), multiquadric (MQ), piecewise linear (PL), and weighted mean (WM) transformations. Their study showed that PL performs

better than TPS and MQ when tie points are sparsely distributed and WM performs better than the others when it contains a large number of tie points and the tie points have positional errors. As the geometric position of pixels changes, the grey values at the vacated grid positions need to be calculated. Metternicht and Zinck [2], Temesgen et al. [3], Hervás et al. [4] and Chen et al. [11] used nearest neighbour interpolation and Vassilopoulou et al. [7] used bilinear interpolation for the resampling process.

Yu et al. [12] proposed satellite image registration technique which performs a pre-registration process that coarsely aligns the input image to the reference image by automatically detecting their matching points by using the scale invariant feature transform (SIFT) method and an affine transformation model. Once the coarse registration is completed, it performs a fine-scale registration process based on a piecewise linear transformation technique using feature points that are detected by the Harris corner detector. Yamaguchi et al. [13] developed two different algorithms to register landslide images with sub-pixel accuracy: the "imageodetic" method and the parabolic function method. In the imageodetic method, bilinear interpolation is used to generate a sub-pixel image by interpolating the values of the original pixels while maximising the correlation coefficient until the sub-pixel accuracy becomes 1/128 of the image resolution. In the parabolic function method, they used a parabolic function to model the correlation coefficient around its peak and from it they locate the position of the peak with sub-pixel accuracy. They used these algorithms to detect a landslide movement as geometric misregistration between two image data of different acquisition dates.

In this paper, an image registration method which is inhomogeneous to account for the local deformations of the terrain, and allows the registration of images with sub-pixels accuracy will be presented. The algorithm is fully automated and it does not rely on the identification of features. Section 2 presents methodology of the elastic image registration algorithm. Section 3 presents the study area and image pre-processing. Section 4 presents choice of parameter values. Section 5 presents results and discussion, and finally, the conclusions will be presented in section 6.

2. Methodology

The purpose of elastic image registration is to detect small local changes, so the proposed method is used to refine global registration already performed. Two images, one before (B) and one after (A) the landslides captured by the same sensor both geocoded and coregistered are assumed to be available. Starting from image B, a sequence of deformed images denoted by $B_1, B_2, B_3, \ldots, B_l$ is created. Each image in the sequence is more similar to image A than the previous one. Each image is created from the previous by applying to it one of the four deformation operators chosen at random and applied at a random position. As the image is deformed, the grey values at integer locations are calculated using the nearest neighbour interpolation rule. If the imposed deformation improves the similarity with the second image, the change it creates is accepted. If it does not, it is rejected and another operator is invoked. The process stops when the deformed image is sufficiently similar with image A. In order to distort image B, four mathematical models of landslides deformation has been developed and used as the transformation operators. These operators imitate deformations expected to be observed when a landslide occurs.

2.1. Exponential growth operator

This operator will deform the grid outwards from a central point, as if material is pouring out of a centre. If the exponential growth operator is chosen, one pixel *i* is randomly chosen as an origin. All other pixels, *k*, will be moved directly away from that pixel by a distance defined by:

$$d_k = re^{-gd_{ik}}, \qquad (1)$$

where *r* and *g* are some parameters and d_{ik} is the distance of pixels *k* from *i*. Changes in pixel location are shown in figure 1(a). In this figure, $P(x_0, y_0)$ is the original pixel location at a distance d_{ik} from *i*, d_x is the distance between *i* and $P(x_0, y_0)$ along the *x*-axis, d_y is the distance between *i* and $P(x_0, y_0)$ along the *y*-axis. $P'(x_0', y_0')$ is the new pixel location of $P(x_0, y_0)$ after deformation i.e. shifted by a distance d_k from $P(x_0, y_0)$ away from *i*, $d_{x'}$ is the distance between $P(x_0, y_0)$ and $P'(x_0', y_0')$ along the *x*-axis and $d_{y'}$ is the distance between $P(x_0, y_0)$ and $P'(x_0', y_0')$ along the *y*-axis. Therefore, the new coordinate of $P'(x_0', y_0')$ are:

$$x_0' = x_0 + \frac{d_x}{d_{ik}}(re^{-gd_{ik}}), \qquad (2)$$

$$y_0' = y_0 + \frac{d_y}{d_{ik}}(re^{-gd_{ik}}). \qquad (3)$$

The effects of this operator in a regular 45 x 45 grid when *i* = (23,23), *r* = 2 and *g* = 0.01 are shown in figure 1(b).

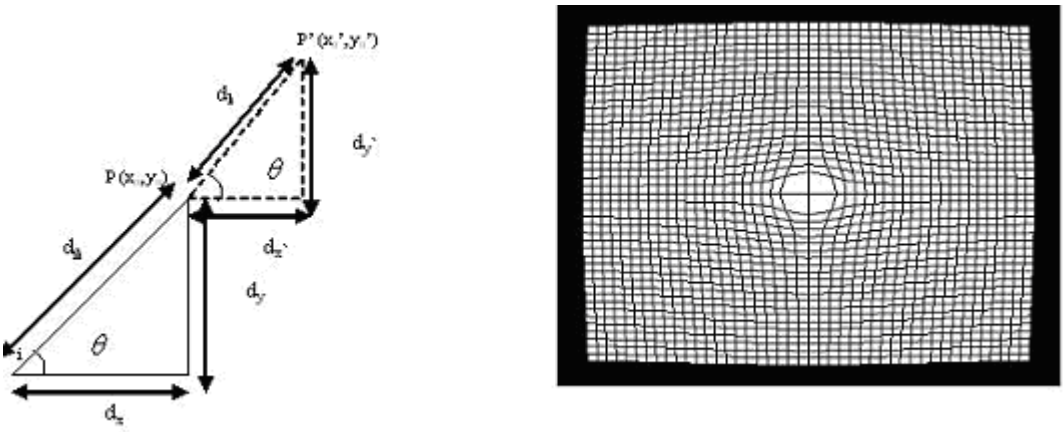

(a) (b)

Figure 1. Exponential growth operator. (a) Changes in the pixel locations. (b) Effects of the exponential growth operator in a regular 45 x 45 grid when *i* = (23, 23), *r* = 2 and *g* = 0.01.

2.2. Exponential shrinkage operator

This operator will deform the grid inwards, towards a central point, as if material is lost into a sink. If the exponential shrinkage operator is chosen, one pixel *i* is randomly chosen as an origin. Instead of moving away from the pixel origin, now all other pixels, *k*, will be moved directly towards that pixel by a distance defined by equation (1). Therefore, by referring figure 2(a), the new coordinates of the pixels are defined as:

$$x_0' = x_0 - \frac{d_x}{d_{ik}}(re^{-gd_{ik}}) \text{ ,} \qquad (4)$$

$$y_0' = y_0 - \frac{d_y}{d_{ik}}(re^{-gd_{ik}}) \text{ .} \qquad (5)$$

Effects of this operator in a regular 45 x 45 grid when i = (23, 23), r = 2 and g = 0.01 shown in figure 2(b).

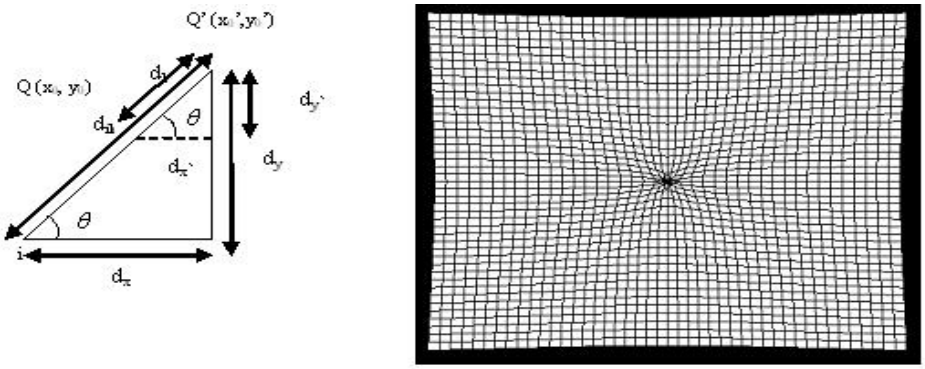

(a) (b)

Figure 2. Exponential shrinkage operator. (a) Changes in the pixel locations. (b) Effects of the exponential shrinkage operator in a regular 45 x 45 grid when i = (23, 23), r = 2 and g = 0.01.

2.3. Exponential translation operator

This operator is relevant for modeling the movement of material during a landslide as chasms and gaps may be opened in the surface of the earth. If the exponential translation operator is chosen, one pixel *i* is randomly selected as an origin. Then, a distance d_{ij}, an orientation θ and the springiness parameter that controls the severity of this distortion, s will be chosen at random. All the remaining pixels, *k*, will be moved directly away from that pixel by a distance defined by:

$$d_k = d_{ij}e^{-sd_{ik}} \text{ ,} \qquad (6)$$

where d_{ik} is the distance between *i* and *k*. Changes in pixel location are shown in figure 3(a). From this figure, $R(x_0, y_0)$ is the original pixel location at a distance d_{ik} from *i*, d_x is the distance between *i* and other pixel, *j* along the *x*-axis, d_y is the distance between *i* and *j* along the *y*-axis. $R'(x_0', y_0')$ is the new pixel location of $R(x_0, y_0)$ after deformation, $d_{x'}$ is the

distance between $R(x_0, y_0)$ and $R'(x_0', y_0')$ along the *x*-axis, and $d_{y'}$ is the distance between $R(x_0, y_0)$ and $R'(x_0', y_0')$ along the *y*-axis. Therefore, the new coordinate of $R'(x_0', y_0')$ are:

$$x_0' = x_0 + d_x e^{-sd_{ik}}, \qquad (7)$$

$$y_0' = y_0 + d_y e^{-sd_{ik}}. \qquad (8)$$

Effects of this operator in a regular 45 x 45 grid when s = 0.1, i = (20,20) and j = (30,30) is shown in figure 3(b).

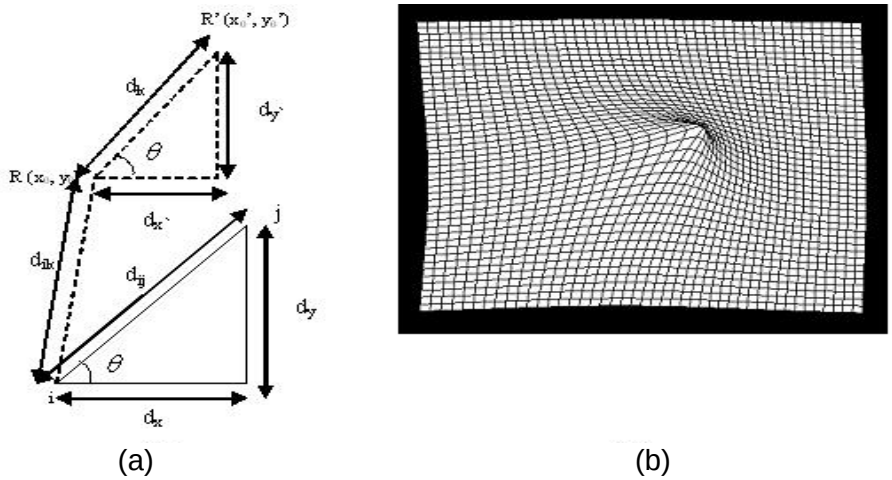

Figure 3. Exponential translation operator. (a) Changes in the pixel locations. (b) Effects of the exponential translation operator in a regular 45 x 45 grid when s = 0.1, i = (20,20) and j = (30,30).

2.4. Exponential parabolic flow front operator

This operator will deform the grid as if a slowly moving parabolically shaped flow front propagates along some direction. Therefore, it is defined for a landslide front originating on an axis *u* moving the material along an orthogonal direction *v*, on some *(u,v)* coordinate system (see figure 4(a)). The following parameters will be chosen: the origin of the deformation, (x_0, y_0), the extent of the deformation, *a*, the severity of the deformation, *b,* the orientation of the deformation, θ, the direction of the deformation, *w,* and the decaying parameter, *t*. When this operator is chosen, one pixel, *i*, at location (x_0, y_0) is selected randomly as the landslide origin. The position of every pixel *k* in the image is then defined in terms of the new origin (x_0, y_0):

$$(x_k', y_k') = (x_k - x_0, y_k - y_0). \qquad (9)$$

The position of pixel *k* in the rotated *(u, v)* coordinate system is defined as follows:

$$u_k' = x_k' \cos\theta + y_k' \sin\theta, \qquad (10)$$

$$v_k' = y_k' \cos\theta + x_k' \sin\theta, \qquad (11)$$

where θ is the orientation of the deformation selected at random. A random number *w* either +1 or -1 is chosen to decide whether the material moves in the anticlockwise or the clockwise direction, respectively. If the pixel satisfies the conditions of $(-a \le u_k' \le +a)$ and

$v_k' w \geq 0$, it will be shifted to the new position, $(u_k, v_k) \equiv (u_k', v_k' + wv')$ where v' is given by equation (12).

$$v' = \frac{b}{a^2}(a^2 - u_k'^2)e^{-t|v_k'|} . \qquad (12)$$

Here, t is defined as the decaying parameter. Otherwise, $(u_k, v_k) \equiv (u_k', v_k')$. The maximum displacement occur when the value of $v_k' = 0$. Finally, the position of the pixel in the *(x, y)* coordinate system is calculated as follows:

$$x_{k_{new}} = u_k \cos\theta - v_k \sin\theta , \qquad (13)$$

$$y_{k_{new}} = u_k \sin\theta + v_k \cos\theta . \qquad (14)$$

Effects of this operator in a regular 45 x 45 grid when x_0= 23, y_0 = 23, a = 5, b = 3, t = 0.1, w = 1 and $\theta = 45^o$ is shown in figure 4(b).

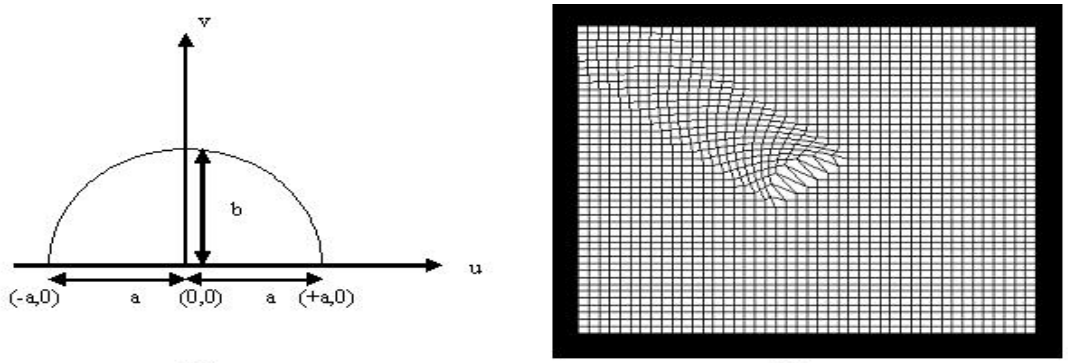

(a) (b)

Figure 4: Exponential parabolic flow front operator. (a) Pixel origin with the shifting parameters *a* and *b.* (b) Effects of the exponential parabolic flow front operator in a regular 45 x 45 grid when x_0= 23, y_0 = 23, a = 5, b = 3, t = 0.1, w = 1 and $\theta = 45^o$.

The cost function that expresses the quality of registration between images A and B_l is defined as follows:

$$U = U_1 + \beta U_2 + \lambda U_3 . \qquad (15)$$

In this expression, β and λ are parameters controlling the relative importance of each term. The three terms combined are the following:

$$U_1 \equiv 1 - S(A, B_l) , \qquad (16)$$

where $S(A, B_l)$ is the measure of similarity between the two images expressed by the correlation coefficient or the mutual information between the two images. The correlation coefficient is defined as in equation (17).

$$R(A, B_l) \equiv \frac{\sum_{i \in T_{A,l}} (p_i^A - \overline{p}^A)(p_i^l - \overline{p}^l)}{\sqrt{\sum_{i \in T_{A,l}} (p_i^A - \overline{p}^A)^2 \sum_{j \in T_{A,l}} (p_j^l - \overline{p}^l)^2}} , \qquad (17)$$

where $T_{A,l}$ represents the overlapping set of pixels of the two images, p_i^A is the pixel value in the first image, p_i^l is the pixel value in the second image, $\overline{p}^A$ is the mean value of the first image and $\overline{p}^l$ is the mean value of the second image, both computed over the overlapping part. For the case of mutual information, $S(A,B_l)$ is equal to $\frac{M_{A,B_l}}{M_{A,A}}$, where M_{A,B_l} is the value of the mutual information between images A and B_l, and $M_{A,A}$ is the entropy of the reference image. The mutual information is defined as follows:

$$M_{A,B} = \sum_{p^A} \sum_{p^B} P_{AB}(p_i^A, p_i^B) \log\left(\frac{P_{AB}(p_i^A, p_i^B)}{P_A(p^A) P_B(p^B)} \right), \quad (18)$$

where $P_A(p^A)$ is the normalised histogram of grey values of the reference image, $P_B(p^B)$ is the normalised histogram of grey values of the sensed image and $P_{AB}(p_i^A, p_i^B)$ is the normalised joint histogram of the grey values p_i^A and p_i^B which correspond to the same pixel *i*.

The second term in equation (15) expresses the desire for image B_l to be distorted as little as possible to fit image A. It is a purely geometric term that does not involve any pixel values:

$$U_2 \equiv \frac{1}{N_{A,l}} \sum_{k \in T_{A,l}} (|x_{k+1} - x_k - d_{xx}| + |y_{k+1} - y_k - d_{xy}| + |x_{k+N_x} - x_k - d_{yx}| + |y_{k+N_x} - y_k - d_{yy}|). \quad (19)$$

Here N_x and N_y is the size of the image along the x and y axes respectively, $N_{A,l}$ is the number of pixels in $T_{A,l}$ and $d_{\alpha,\beta}$ is the difference in the coordinate along the β axis in two neighbouring pixels "aligned" along the α axis. In a regular grid, $d_{xx} = d_{yy} = 1$ and $d_{xy} = d_{yx} = 0$. Note that k scans the image in a raster fashion, along the x axis on each successive line corresponding to fixed y. More explicitly, the meaning of this term in this function may be understood by the following example: x_{k+1} and x_k are the coordinate positions along the x axis of the two neighbouring pixels with indices $k + 1$ and k respectively. At the beginning of the iterative process, the difference between these two coordinates is d_{xx} since these pixels are next to each other along the x axis. After an iteration take place, the two pixels may shift with respect to each other, so their distance along the x axis may have changed. The difference between this distance and the original value d_{xx} expresses the distortion of the rigid grid. In a similar way, term $|x_{k+N_x} - x_k - d_{yx}|$ expresses the distortion of the grid away from the rigid one, due to the shifting in relative position of two neighbouring pixels along the y axis (indices $k+N_k$ and k identify neighbouring pixels along the y axis in the raster indexing format).

Finally, the third term of the cost function expresses the desire for maximum overlap between images A and B_l defined in equation (20).

$$U_3 \equiv 1 - \frac{N_{A,B_l}}{N} \quad . \quad (20)$$

Here N is the maximum number of pixels in an image, and N_{A,B_l} is the number of pixels in the overlapping part of images B_l and A.

3. Imagery used

The proposed elastic image registration technique has been used to detect landslide events in Caramanico, Italy. A pair of sub-images taken from the 1998-1999 landslide events in Caramanico as shown in Figures 5(g)-(h) were used as the training dataset. Three other pairs of sub-images of the landslide events in Caramanico were used as the testing datasets. They were taken from the 1995-1996 landslide events as shown in Figures 5(a)-(b), from the 1996-1997 landslide events as shown in Figures 5(c)-(d), and from the 1997-1998 landslide events as shown in Figures 5(e)-(f). Before performing an elastic image registration, the images were preprocessed to remove clouds and snowed mountain peaks by using the cloud-snow detection algorithm proposed by Hou et al. [14]. The Principal Component Analysis (PCA) was then used to produce a grey band with maximum contrast.

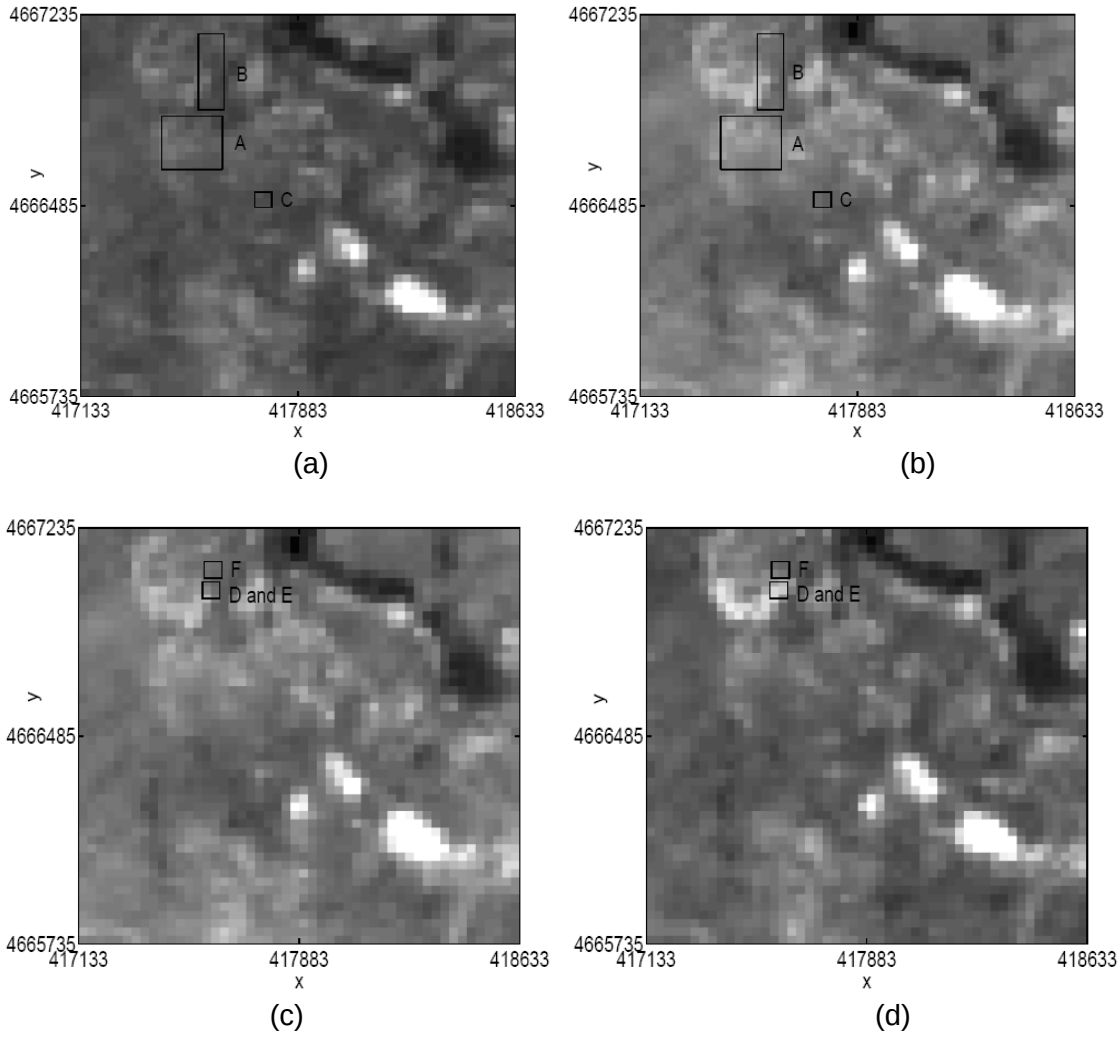

Figure 5: Landslide sub-images in Caramanico. (a) 1995-1996 events. (Image dated 17/6/1995.) (b) 1995-1996 events. (Image dated 18/5/1996.) (c) 1996-1997 events. (Image dated 18/5/1996.) (d) 1996-1997 events. (Image dated 21/5/1997.)

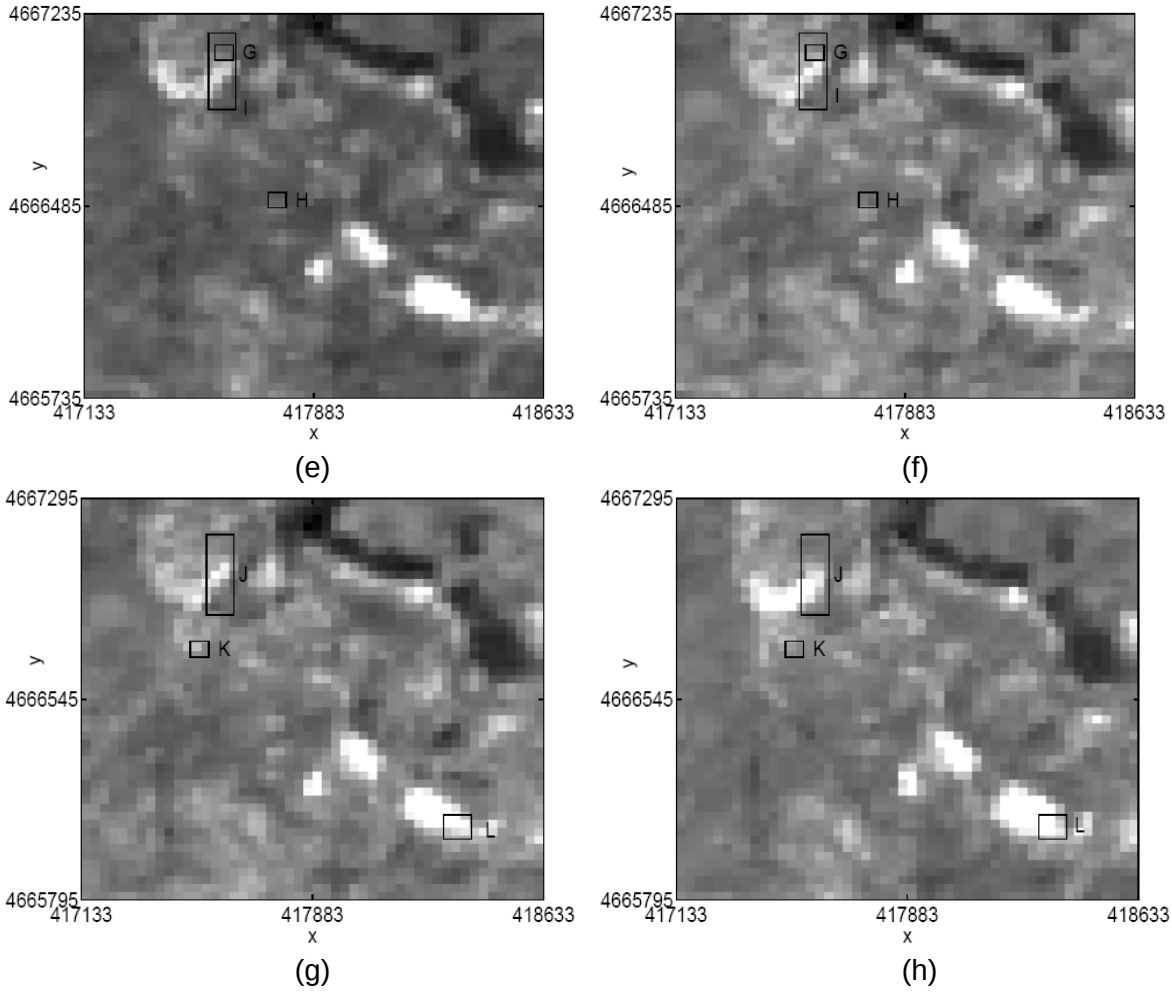

Figure 5 (continue.): Landslide sub-images in Caramanico. (e) 1997-1998 events. (Image dated 21/5/1997.) (f) 1997-1998 events. (Image dated 22/4/1998.) (g) 1998-1999 events. (Image dated 22/4/1998.) (h) 1998-1999 events. (Image dated 27/5/1999.)

4. Choice of parameter values

4.1. Parameters of the operators

The satellite images available for the experiments have already been globally registered and they only suffer from small deformations. Therefore, only parameter settings that produce small movements and thus can be used to detect small local changes will be considered. In order to have only sub-pixel shifts, the maximum movement of one pixel will be allowed. Then, in order to avoid larger shifts, the value of parameter r for the growth and shrinkage operator is fixed to 2, and the value of parameters d_{ij} and b for the translation and parabolic front flow operators is fixed to 1. Different combinations of parameters will have different decaying rates of shifting. Any shift smaller than 0.05 pixels will be neglected. Therefore, any parameter values that shift the pixels by less than 0.05 pixels from the seed pixel will not be used. In order to

have only local deformations, any shift outside a 9 × 9 local window will be neglected. We can see from Figure 6 that for the parameter values considered in these graphs, neglecting any shift outside a local window is consistent with keeping shifts of size greater or equal to 0.05. In addition, parameter values which at distance 4 pixels away from the seed point that create shifts greater than 0.05 will not be considered. As a result, for the exponential growth and shrinkage operator, parameters r was fixed to 2, while parameter g was chosen from a uniform distribution in the range of [0.8 2.0]. For the exponential translation operator, parameter d_{ij} was fixed to 1, while parameter s was chosen from a uniform distribution in the range of [0.6 2.0]. For the exponential flow operator, parameter t was chosen from a uniform distribution in the range of [0.6 2.0], parameter a was chosen from a uniform distribution in the range of [1 3], while parameter b was fixed to 1.

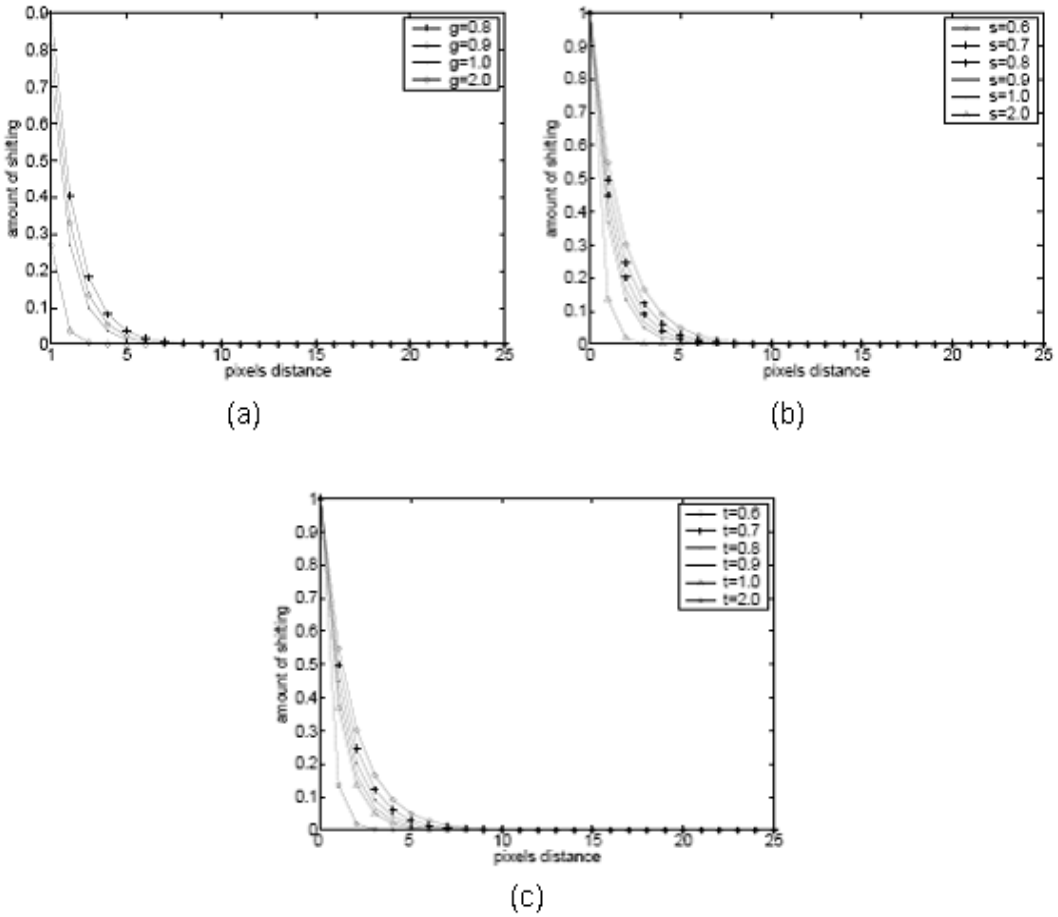

Figure 6: Shifting induced by the various operators. (a) Exponential growth and shrinkage operator with $r = 2$, $g \in [0.8, 2.0]$. (b) Exponential translation operator with $d = 1$, $s \in [0.6, 2.0]$. The value of parameter t is irrelevant here. (c) Exponential parabolic flow front operator with $b = 1$ and $t \in [0.6,2.0]$ at $u_k = 0$. The value of parameter a and θ are irrelevant here.

4.2. Stopping criterion

The acceptance of a proposed deformation is controlled by the value of the cost function. If it reduces the value of he cost function, the deformation is accepted. The algorithm stops when the value of the cost function after each 10 000 tries changes by no more than 1%. The relative change of the value of the cost function is calculated as follows:

$$c \equiv \frac{c_a - c_{a+1}}{c_a} \times 100\%, \qquad (21)$$

where c_a and c_{a+1} are the values of the cost function in two successive estimates one hundred thousand tries apart.

4.3. Parameter β and λ

The quality of registration between two images is controlled by the cost function, which consists of three terms. Therefore, the optimal values of the coefficients which linearly combined to form the cost function need to be identified. In order to find the values of β and λ, the exploratory run for various parameter settings has been performed. Mutual information is used to evaluate the quality of registration obtained for each set of parameter values. The set of values of parameters β and λ that gives the highest value of mutual information will be used in the full runs performed later. As a result, the parameter β was fixed to 0.005 and λ to 0.1 when the correlation coefficient was used as the similarity measure in the cost function. When the mutual information was used as the similarity measure in the cost function, the parameter β was fixed to 0.0007 and λ to 0.7.

5. Results and discussion

The process of image registration deformed the image taken before the landslides to match the image after the landslides. Here, the parameter settings of section 4 have been used to register the landslide images 25 times with a different seed each time for the random number generator. This method was developed in two versions. One version using the correlation coefficient as a similarity measure of the grey level values between two images and the other version using mutual information for the same purpose. From Figure 7, we can see that the exponential parabolic flow front operator gave the highest percentage of acceptance during the exploratory run in the both version. This is because this operator imitates best what happens during a landslide.

Figure 8 shows the 2% most significant shifts for average vectors, $(\overline{s_x}(i,j), \overline{s_y}(i,j))$ for registration based on the correlation function and also based on the mutual information. From this figure, we can see that the 2% most significant shifts are less localized when the correlation function was used than the mutual information. The second way to compare the two approaches is to check how close to reported landslides the identified regions of significant shifts are located. Figures 9 and 10 show all identified peaks numbered in order of significance. To assess the quality of the result, the distance between the centers of the recorded landslide areas from the nearest identified peaks in these shift maps has been calculated. The results are shown in Tables 1 and 2. From these tables, we can see that the mutual information-based method not only indicates that the significant total shifts are nearer to the marked locations of the landslides (smaller distances), but also that these are the

strongest peaks (higher order peaks, e.g. 3 instead of 6) in the shift maps. Since the mutual information based method gave more reliable results, therefore, this method was then used to register three other pairs of landslide images. The images are taken from the 1995-1996, 1996-1997 and 1997-1998 landslide events in Caramanico.

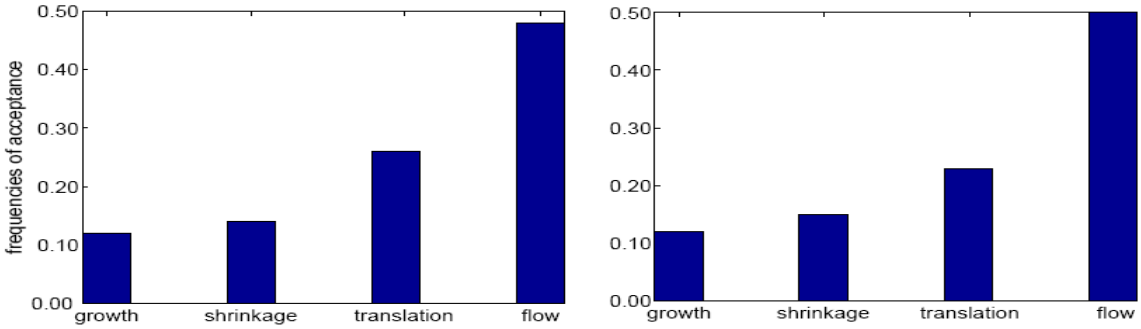

Figure 7. Frequencies of acceptance of the changes proposed by the various operators. Correlation coefficient as the similarity measure in the cost function. (b) Mutual information as the similarity measure in the cost function.

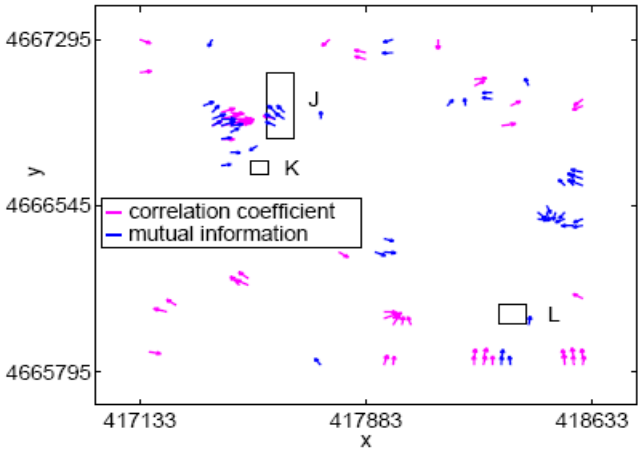

Figure 8. The 2% most significant shifts: vectors $(\overline{s_x}(i,j),\overline{s_y}(i,j))$ based on the correlation coefficient (in magenta colour) and vectors $(\overline{s_x}(i,j),\overline{s_y}(i,j))$ based on mutual information (in blue colour).

The range of values of movement within the boxes, indicating the locations of the reported landslides, and around the identified corresponding locations were calculated and compared with the reported values. In some cases, the size of the reported movement was not given numerically. Only linguistic terms were used. Therefore, the size of movement in these areas was inferred by referring to the meaning of the terms that were used in the other cases. Terms like "mudslide movement", "shallow earthflow" or "slow debris flow" were used in cases *A, C, F, G, H* and *K*. Only in case *A* the movement was given as being of at least 10*m*. So, the movement in cases *C, F, G, H* and *K* was assumed to be also the same order of magnitude. Cases *B, I* and *J* are rotational slides. For case *B* the size of the movement was given to be about 80*m* to a few hundred meters. Therefore, the size of the movement in cases *I* and *J* was

assumed to be also the same order of magnitude. The results are summarised in Table 3 for the 1998-1999 landslide events and Table 4 for the 1995-1996, 1996-1997 and 1997-1998 landslide events. Overall, the amount of movements around the identified landslide locations is in general agreement with the amount of reported movement. Only in three cases where the movement was reported to be of a few hundred meters the results are not consistent. From these results, we conclude that the algorithm can be used to detect and quantify landslide movements with the value of few tenth of meters.

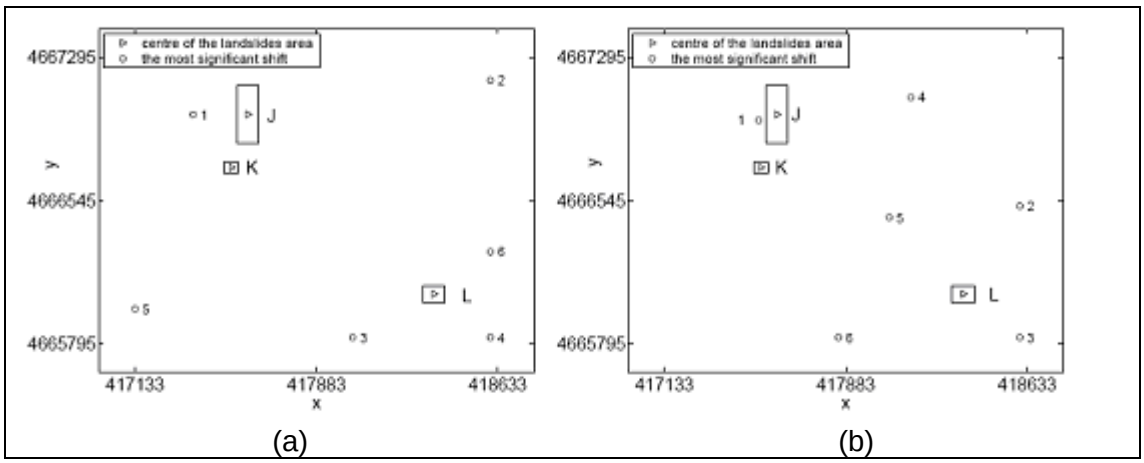

Figure 9. All identified peaks from the significant shifts in 25 runs. (a) Results when the correlation coefficient is used as the similarity measure in the cost function. (b) Results when mutual information is used as the similarity measure in the cost function.

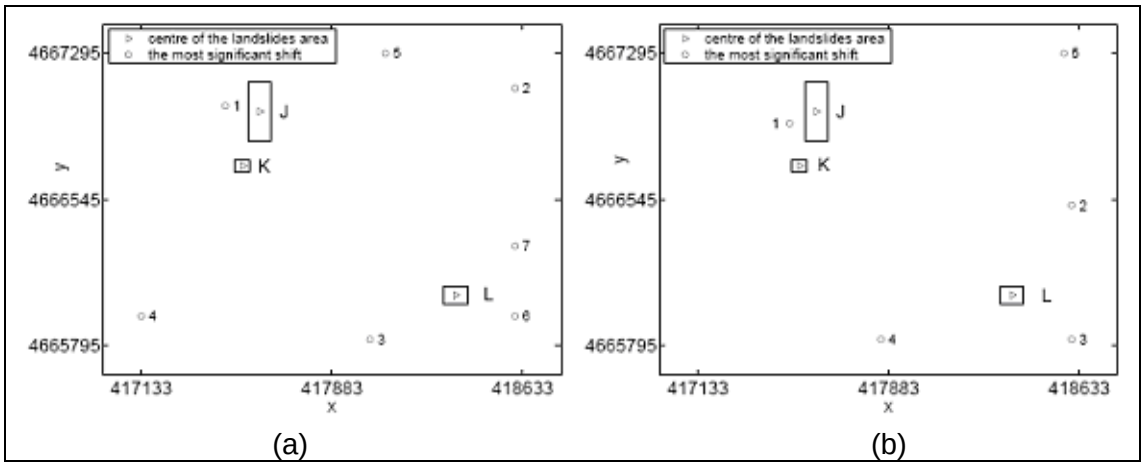

Figure 10. All identified peaks from the average total shifts in 25 runs. (a) Results when the correlation coefficient is used as the similarity measure in the cost function. (b) Results when mutual information is used as the similarity measure in the cost function.

Table 1. Location of the nearest peaks to the landslide area based on the significant shifts. (Please refer to Figure 9.)

Landslide	Measure of similarity	Nearest peak	Distance (pixel)
J	Correlation function	1	7.5300
	Mutual information	1	2.7346
K	Correlation function	1	10.6720
	Mutual information	1	8.2700
L	Correlation function	6	10.7510
	Mutual information	3	10.8827

Table 2. Location of the nearest peaks to the landslide area based on the average shifts. (Please refer to Figure 10.)

Landslide	Measure of similarity	Nearest peak	Distance (pixel)
J	Correlation function	1	4.6310
	Mutual information	1	4.0760
K	Correlation function	1	10.5185
	Mutual information	1	7.3795
L	Correlation function	6	8.5834
	Mutual information	3	10.8827

Table 3. Comparison between the inferred or reported movement and the detected range of values of the movement for 1998-1999 landslide events.

Events	Case	Reported size, (*m*)	Inside box, (*m*)		Nearest peak, (*m*)		
			Correlation function	Mutual information	Correlation function	Mutual information	
1998-1999	J	80-300	3.43-43.29	4.73-40.89	10.24-90.89	1.97-42.41	×
	K	more than 10	7.74-20.92	4.65-20.09	10.65-48.88	3.93-32.05	√
	L	more than 10	6.33-22.62	8.93-27.18	10.23-28.86	15.74-28.60	√

Table 4. Comparison between the inferred or reported movement and the detected range of values of the movement for 1995-1998 landslide events.

Events	Case	Reported size, (*m*)	Inside box, (*m*)	Nearest peak, (*m*)	
1995-1996	A	10-200	3.14-24.76	1.52-22.50	√
	B	80-300	1.57-25.01	1.97-22.50	×
	C	more than 10	5.32-20.91	6.30-25.16	√
1996-1997	D	25	4.15-23.32	3.27-29.47	√
	E	30	4.15-23.32	3.27-29.47	√
	F	more than 10	9.85-23.24	3.27-29.47	√
1997-1998	G	more than 10	23.61-42.22	4.94-25.36	√
	H	more than 10	3.43-20.01	6.14-15.69	√
	I	80-300	0.30-42.22	4.94-32.83	×

6. Conclusions

In this paper, a new method of landslide detection and quantification based on elastic image registration has been presented. The method does not rely on any parametric model of image transformation, e.g. affine transform, and can be used to register images with sub-pixel accuracy even when the distortion suffered by one of them is totally inhomogeneous and highly localized. There are two versions of the method. One used the correlation function as a measure of similarity and the other used the mutual information. Four mathematical models of landslide deformation have been developed and used as the transformation operator in the image to image registration process. It was concluded that the exponential polynomial operator was the most useful of all. This is validated by the ground information, according to which, in almost all cases the landslides were caused by rotational type of movement. The size of detected movement is depends on the selection of setting parameters in the deformation operators and stopping criterion. The quality of the results was assessed by checking the consistency and repeatability of the results, repeating each experiment 25 times with a totally different sequence of the deformation operators including different parameter values, all chosen at random. From the results, it was concluded that mutual information not only gave consistent results for the 2% most significant shifts, but also gave more localized average shift vectors. In terms of the average significant local shift, the mutual information gave the best agreement with the reported locations of the landslides. From the results, it can be concluded that the elastic image registration can be used to monitor the landslide movement with sub-pixel accuracy even when the distortion suffered by one of them is totally inhomogeneous and highly localized. Therefore, it can be used to improve the capability of coarse spatial resolution satellite

images and thus can be used to monitor and quantify landslide movement with sub-pixel accuracy. However, the main drawback of this approach is that it does not include a mechanism that allows the distinction between a landslide and any other change on the surface of the Earth that caused the change in the appearance of the image. Such a mechanism should probably involve higher level knowledge, multispectral information and it should probably operate in conjunction with an expert system.

7. References

[1] L.G. Brown, "A survey of image registration techniques", ACM Computing Surveys 24(4)(1992), pp. 325-376.
[2] G.I. Metternicht, and J.A. Zinck, "Evaluating the information content of JERS-1 SAR and Landsat TM data for discrimination of soil erosion features", ISPRS Journal of Photogrammetry and Remote Sensing 53(1998), pp. 143-153.
[3] B. Temesgen, M.U. Mohammed, and T. Korme, "Natural hazard assessment using GIS and remote sensing methods, with particular reference to the landslides in Wondogenet Area, Ethiopia", Phys. Chem. Earth (C) 26(9)(2001), pp. 665-675.
[4] J. Hervás, J.I.. Barredo, P.L. Rosin, A. Pasuto, F. Mantovani, and S. Silvano, "Monitoring landslides from optical remotely sensed imagery: the case history of Tessina landslide, Italy", Geomorphology 1346(2003), pp. 1-13.
[5] A. Kääb, "Monitoring high mountain terrain deformation from repeated air- and spaceborne optical data: examples using digital aerial imagery and ASTER data", ISPRS Journal of Photogrammetry and Remote Sensing 57(2002), pp. 39-52.
[6] P. Mora, P. Baldi, G. Casula, M. Fabris, M. Ghirotti, E. Mazzini, and A. Pesci, "Global Positioning System and digital photogrammetry for the monitoring of mass movements: application to the Ca' di Malta landslide (northern Appennis, Italy)", Engineering Geology 68(2003), pp. 103-121.
[7] S. Vassilopoulou, L. Hurni, V. Dietrich, E. Baltsavis, M. Pateraki, E. Lagios, and I. Parcharidis, "Orthophoto generation using IKONOS imagery and high-resolution DEM: a case study on volcanic hazard monitoring of Nisyros Island (Greece)", ISPRS Journal of Photogrammetry and Remote Sensing 57(2002), pp. 24-38.
[8] K. Honda, and M. Nagai, "Real-time volcano activity mapping using ground-based digital imagery", ISPRS Journal of Photogrammetry and Remote Sensing 57(2002), pp. 159-168.
[9] B. Casson, C. Delacourt, D. Baratoux, and P. Allemand, "Seventeen years of the La Clapiere landslide evolution analysed from ortho-rectified aerial photographs", Engineering Geology 68(2003), pp. 123-139.
[10] L. Zagorchev, and A. Goshtasby, "A comparative study of transformation functions for nonrigid image registration", IEEE Transactions on Image Processing 15(2006), pp. 529–538.
[11] C.M. Chen, G.F. Hepner, and R.R. Foster, "Fusion of hyperspectral and radar data using the HIS transformation to enhance urban surface features", ISPRS Journal of Photogrammetry and Remote Sensing 1236(2003), pp. 1-3.
[12] L. Yu, D. Zhang, and H. Eun-Jung, "A fast and fully automatic registration approach based on point features for multi-source remote-sensing images", Computers & Geosciences 34(2008), pp. 838-848.
[13] Y. Yamaguchi, S. Tanaka, T. Odajima, T. Kamai, and S. Tsuchida, "Detection of a landslide movement as geometric misregistration in image matching of SPOT HRV data of two different dates", Int. J. Remote Sensing preview article (2002), pp. 1-12.
[14] P. Hou, M. Petrou, C. Underwood, and A. Hojjatoleslami, "Improving JPEG performance in conjunction with cloud editing for remote sensing applications", IEEE Transactions on Geoscience and Remote Sensing 38(2000), pp. 515-524.